

# A High-resolution Microcavity Transmission Spectrometer

Ruocan Zhao<sup>1†</sup>, Bin Yang<sup>1†</sup>, Chuan Huang<sup>1</sup>, Jiangtao Li<sup>1</sup>, Baoqi Shi<sup>3</sup>, Wei Sun<sup>3</sup>, Chen Shen<sup>3,4</sup>, Chong Wang<sup>1</sup>, Tingdi Chen<sup>1,2</sup>, Chen Liang<sup>2</sup>, Xianghui Xue<sup>1,2,5,6</sup>, Junqiu Liu<sup>2,3</sup>, Xiankang Dou<sup>2</sup>

\*Corresponding author. Email: [xuexh@ustc.edu.cn](mailto:xuexh@ustc.edu.cn)

1. CAS Key Laboratory of Geospace Environment, School of Earth and Space Sciences, University of Science and Technology of China, Hefei 230026, China

2. Hefei National Laboratory, University of Science and Technology of China, Hefei 230088, China

3. International Quantum Academy, Shenzhen 518048, China

4. Qaleido Photonics, Shenzhen 518048, China

5. CAS Center for Excellence in Comparative Planetology, Anhui Mengcheng Geophysics National Observation and Research Station, University of Science and Technology of China, Hefei, China

6. Hefei National Research Center for Physical Sciences at the Microscale and School of Physical Sciences, University of Science and Technology of China, Hefei, China.

†These authors contributed equally to this work

**Abstract:**

Spectral analysis is one of the most powerful tools for studying and understanding matter. As a key branch, absorption spectroscopy is widely used in material detection, isotope analysis, trace gas detection, and the study of atomic and molecular hyperfine structures. Traditional mode-locked optical frequency combs, which feature broad spectra and low repetition rates, have enabled high-precision absorption measurements through dual-comb techniques. These combs have found applications in trace gas detection, spectral imaging, and isotope analysis. However, their complexity, bulkiness, and large size limit their use outside laboratories. In contrast, low-noise optical frequency combs generated by optical micro-resonators offer significant potential advantages for spectroscopy due to their chip-scale size and lightweight design. We present a microcavity-based transmission spectrometer using a single silicon nitride microcavity soliton, achieving a 4 THz bandwidth with 200 kHz resolution. This system combines the stable dissipative Kerr soliton (DKS) comb from a silicon nitride micro-resonator with the dual-sideband scanning from an intensity electro-optic modulator (EOM), transferring sub-Hz RF precision to the optical domain. The resulting frequency-modulated (FM) comb inherits the high precision of the RF domain, with optical accuracy dominated by the pump laser and repetition rate stability. The DKS comb allows independent locking of the pump laser and repetition rate, facilitating ultra-precise FM comb generation. The frequency-modulated comb is then imaged onto a 2D CCD array using a VIPA in tandem with a diffraction grating, enabling the recording of a composite spectrum during scanning. It is anticipated that using an ultra-

narrow linewidth laser locked to an ultra-stable cavity as the pump source could enable Hz-level precision and stability. Given the integration advantages of the key components in this approach, it holds significant potential for future miniaturization, offering vast possibilities for compact, high-precision spectroscopic measurements.

## **Introduction**

Self-referenced optical frequency combs (OFCs) based on femtosecond pulse lasers use the dual-comb technique to bridge the optical domain with the RF or microwave domain<sup>1-4</sup>. These mode-locked lasers, which span frequencies from the extreme ultraviolet to the mid-infrared, can be locked to reference sources such as atomic clocks or stable reference cavities. This capability has revolutionized optical metrology and spectroscopy<sup>5-9,36</sup>. However, despite their excellent performance and widespread success in these fields, the large size, high power consumption, and complex, precise structure of mode-locked laser-based OFCs have constrained their broader adoption.

In recent years, dissipative Kerr soliton optical frequency combs, generated by high-Q microresonators at the chip scale, have gained increasing attention due to their simple structure and miniaturization advantages, sparking significant research and development<sup>10-12</sup>. Dissipative Kerr solitons have been realized in microresonators made from various materials, generating comb-like lines in the frequency domain similar to those produced by mode-locked lasers and generating high-coherence, low-noise femtosecond pulse trains<sup>10,13-18,37</sup>. As a result, soliton microcombs show great promise in applications in optical atomic clocks<sup>19,20</sup>, spectroscopy<sup>21</sup>, distance measurement<sup>22</sup>,

LiDAR<sup>23</sup>, and low-noise microwave sources<sup>12,24,38</sup>. In the field of spectroscopy, high-resolution spectra are typically achieved using traditional mode-locked fiber lasers, either by directly resolving single lines<sup>25</sup> or using dual-comb techniques<sup>4,26</sup>. The frequency resolution in these systems is primarily limited by the spacing of the comb lines. However, the high repetition rate (greater than 10 GHz) of high-Q microresonators pose a limitation for spectroscopy applications<sup>21</sup>. To address this, some research groups have proposed comb spectroscopy techniques based on thermal tuning of the effective cavity length for continuous soliton scanning, thereby overcoming the limitation of low spectral resolution caused by high repetition rates<sup>27–29</sup>. This approach allows for the theoretical determination of the minimum resolution by the linewidth of the comb lines. However, this method requires the pump light to scan at the same speed as the cavity mode to maintain the soliton state. The limited thermal modulation rate restricts the scanning speed, while the need for the pump to track the cavity mode—combined with the instability of the soliton repetition frequency—limits the overall system stability and spectral precision. Additionally, one group has employed external modulation to achieve soliton scanning over a relatively broad range, using dense wavelength division multiplexing (DWDM) to select a single comb line from the soliton comb, followed by single-sideband modulation<sup>30</sup>. Nevertheless, the scanning range still requires further enhancement.

In this work, we propose a novel approach for wide-range continuous soliton scanning. By combining a VIPA with a diffraction grating, the scanned one-dimensional soliton spectrum can be imaged onto a two-dimensional CCD array, enabling fast, high-

precision spectroscopic measurements over a wide range<sup>25,31,32</sup>. External modulation allows the pump light to be independently locked to a reference source, with its repetition frequency stabilized via closed-loop feedback control of pump power<sup>33,34</sup>. This approach enhances soliton stability and brings the system resolution close to the limit of the soliton comb linewidth. As a result, a spectrometer with a resolution of 200 kHz has been achieved. This innovative design provides a promising solution for next-generation compact and ultra-high-resolution spectroscopy.

## Results

**Principle and experimental set-up:** Figure 1 shows the schematic diagram of our microcavity transmission spectrometer. The dissipative Kerr soliton (DKS) comb generated by a silicon nitride microcavity pumped with a single-frequency laser acts as a broadband, highly coherent light source. However, its high repetition rate (low spectral resolution) limits its application in spectroscopic measurements. This limitation can be overcome by introducing an electro-optic intensity modulator. When the DKS comb passes through the modulator, its optical field is shaped by the applied RF electric field. With an appropriate bias voltage, the original DKS comb carrier is suppressed and disappears, while two sidebands are symmetrically generated around it. The spectral spacing between the sidebands and the carrier is determined by the frequency of the applied RF field. When the RF field frequency is swept over time, covering a range up to half the DKS comb's repetition rate, and the resulting spectra are combined, a new comb with a lower repetition rate can be synthesized. This new comb, referred to as a frequency-modulated optical comb, enables high-resolution

spectroscopy, with its spectral resolution determined by the step size of the RF frequency sweep. The frequency-modulated optical comb is then passed through the sample under test, allowing the extraction of the sample's absorption features. At any given moment, the frequency-modulated comb can be viewed as a superposition of two original Kerr soliton combs, with the minimum frequency spacing determined by their relative positions. In most cases, this minimum spacing remains large enough to be resolved by conventional dispersive elements. Here, we utilize a combination of a VIPA and a diffraction grating to map the one-dimensional frequency-modulated comb, after interaction with the sample, onto a two-dimensional space, which is then captured by a CCD array. This approach not only achieves extremely high spectral resolution but also compresses the spectrum into a smaller two-dimensional spatial region. The high spectral resolution ensures maximum comb-tooth distinction, while the one-dimensional to two-dimensional spectral mapping allows for the accommodation of a broader spectrum within a limited spectral range. Although the VIPA and grating combination offer very high spectral resolution, it does not represent the resolution limit of this method. Their primary purpose is to resolve the comb teeth of the frequency-modulated optical comb while enabling broad-spectrum measurement. The ultimate resolution of this method is determined by the stability of the pump laser, the soliton repetition rate, and the linewidth of the comb teeth in the frequency-modulated optical comb.

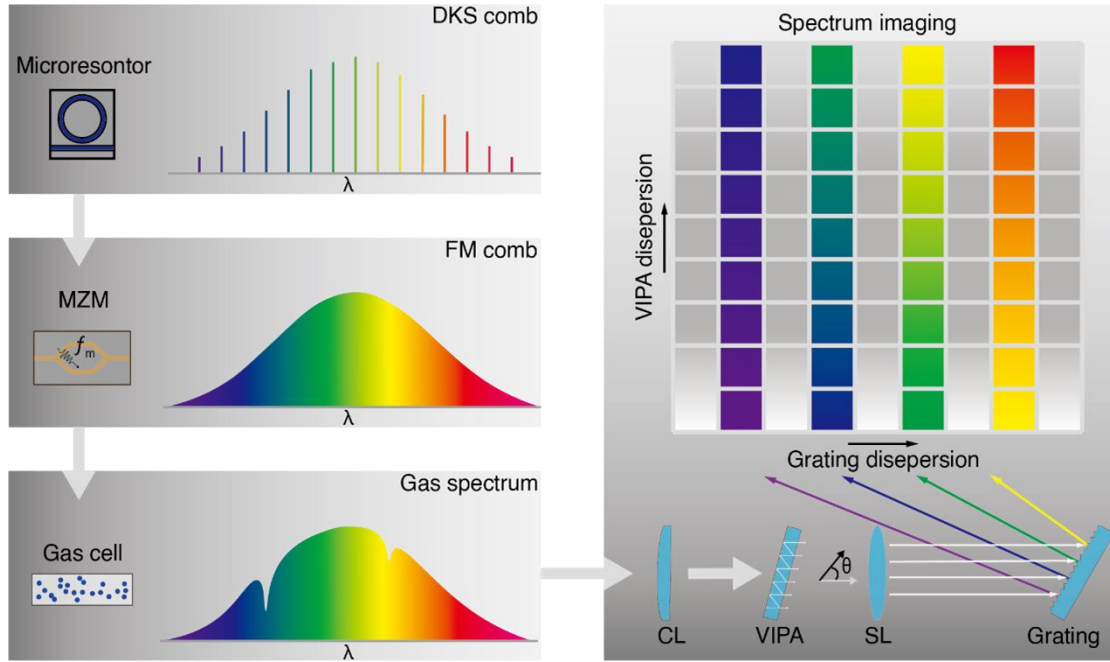


Fig. 1 Schematic Diagram of the Principle of the Microcavity Transmission Spectrometer. MZM: Mach-Zehnder Modulator; FM: Frequency Modulation; CL: Cylindrical Lens; SL: Spherical Lens.

Following this concept, we designed the optical setup shown in Figure 2(a). The pump laser is a continuously tunable laser, amplified to approximately 800 mW using an erbium-doped fiber amplifier, and then coupled into a silicon nitride microresonator. The light exits from the other end of the microresonator and is recoupled into an optical fiber. By sweeping the pump laser frequency with forward and backward tuning methods<sup>35</sup>, the laser can be tuned to a frequency range where a single-soliton state exists, enabling the generation of a dissipative Kerr soliton (DKS) comb, as shown in Figure 2(b). When the temperature of the microresonator is sufficiently stabilized, the single-soliton DKS comb can maintain long-term stability. Once the DKS comb is stably generated, the pump laser is locked to a stable reference Fabry-Pérot (FP) cavity to ensure long-term frequency stability. The DKS comb is then split into two paths using a fiber splitter. The weaker path is sent to a phase-modulated electro-optic modulator

(EOM) with a modulation frequency  $f_{mi} = (f_r - f_m)/2$ , where  $f_r$  is the DKS soliton repetition frequency and  $f_m$  is a reference frequency for locking the repetition rate. Both  $f_m$  and  $f_{mi}$  are traceable to a precise rubidium atomic clock. The modulated signal is then detected by a high-speed photodetector (PD), producing a signal that is mixed with a reference signal of frequency  $f_m$  in a radio-frequency (RF) mixer. After low-pass filtering, the output is processed by a proportional-integral-derivative (PID) controller, which feeds back to an acoustic-optic modulator (AOM) to adjust the power delivered to the microresonator. This feedback mechanism controls the DKS soliton repetition frequency, achieving stable locking of the DKS repetition rate. The stronger path is directly routed into an electro-optic intensity modulator to generate the frequency-modulated comb, as shown in Fig. 2(d). This comb is then split into two branches: one is directed through the device under test, while the other serves as a pure-fiber reference, selected by an optical switch. The two branches are subsequently merged into a single path via another optical switch. (Two optical switches are used to mitigate crosstalk between channels, which can induce phase disturbances; the use of two switches significantly reduces such interference compared to a single switch.) After polarization scrambling using a high-speed polarization scrambler, the frequency-modulated comb is directed into a reflective collimator. The collimator converts the light into a collimated free-space beam with a diameter of approximately 13 mm. The beam is then focused by a two-inch cylindrical lens and sequentially passes through a two-inch dispersive element (VIPA) and a blazed grating. The dispersed light is subsequently focused by an achromatic spherical lens onto a CCD array for imaging.



The high-speed polarization scrambler is placed before the reflective collimator to address the polarization sensitivity of the blazed grating. By scrambling the polarization of the comb at a high rate (700 kHz), the scrambler eliminates the grating's polarization dependence, ensuring more accurate measurement results.

**Generation of the frequency-modulated comb:** A single-frequency continuous-wave laser passes through an intensity-modulated EOM, producing two sidebands on either side of the laser frequency. The intensities of the odd- and even-order optical sidebands can be mathematically expressed as:

$$P_{2n+1} = \frac{1}{2} E_0^2 J_{2n+1}^2(C) [1 - \cos \varphi] \quad (n = 0, 1, 2, \dots), \quad (1)$$

$$P_{2n} = \frac{1}{2} E_0^2 J_{2n}^2(C) [1 + \cos \varphi] \quad (n = 0, 1, 2, \dots), \quad (2)$$

where  $E_0$  represents the incident optical field intensity,  $J_{2n}(C)$  and  $J_{2n+1}(C)$  denote the first-kind  $n$ -th order Bessel functions corresponding to the intensities of the odd- and even-order optical sidebands, respectively.  $C = \pi \frac{V_m}{2V_\pi}$  indicates the modulation depth of the signal,  $V_m$  is the amplitude of the applied RF signal,  $\varphi = \pi \frac{V_{bias}}{2V_\pi}$ , and  $V_{bias}$  represents the applied DC bias voltage. From equations (1) and (2), the intensity of each optical sideband is determined by both the modulation depth and the DC bias. For an intensity-modulated EOM, the strength of each sideband can be adjusted by varying the DC bias without altering the modulation signal, which is a unique feature of frequency shifting via electro-optic intensity modulation. When  $\varphi = (2n+1)\pi$ , the odd-order sidebands reach maximum intensity, while the even-order sidebands are suppressed. In this case, the original carrier component vanishes, leaving the primary frequency components as the first-order sidebands on either side of the carrier. The frequency

separation between the first-order sidebands and the carrier,  $f_m$  is determined by the applied RF frequency. Similarly, if the single-frequency continuous light is replaced with a DKS comb, it can be inferred that when the applied voltage satisfies the  $\varphi = (2n+1)\pi$  condition, the original DKS comb acts as the carrier and its even-order sidebands are suppressed. The remaining frequency components are primarily the first-order sidebands of the DKS comb, effectively separating the original DKS comb into two sub-DKS combs. These sub-DKS combs exhibit a tooth spacing of  $2f_m$ , as illustrated in Figure 2(d). The newly formed sub-DKS combs constitute the frequency-modulated comb. If the modulation frequency  $f_m$  is increased from 0 to  $f_r/2$  in discrete intervals of  $\Delta f$  over a time period  $t$ , a series of frequency-modulated combs corresponding to the modulation frequencies will be generated. By integrating these frequency-modulated combs over the time  $t$ , a new composite comb with a repetition rate of  $f_{step}$  can be obtained. This novel composite comb enhances spectral resolution at the expense of temporal resolution, with its spectral resolution determined by  $f_{step}$ . If this composite comb interacts with a sample during the time  $t$ , the spectral absorption characteristics of the sample can be recorded with a resolution of  $f_{step}$ .

**Design of the VIPA Spectrometer System:** To rapidly detect frequency-modulated combs and record broad spectral information, we employ a combination of a VIPA and a diffraction grating to map the one-dimensional spectrum of the frequency-modulated comb onto a two-dimensional CCD array. This approach enables the simultaneous recording of a broad spectrum with extremely high resolution. The VIPA offers superior spectral resolution compared to a grating; however, for spectra wider than one free

spectral range (FSR), spectral aliasing occurs. By combining the VIPA with a grating, which provides spectral resolution sufficient to resolve beyond one FSR of the VIPA, this aliasing issue is effectively addressed. Using Figure 1 as an example, the VIPA projects its image onto the CCD in the vertical direction. Without a blazed grating in the optical path, a broadband light source would produce a single vertical stripe on the CCD. Each point on this stripe contains light at wavelengths separated by integer multiples  $n$  (0,1,2,...) of the FSR. Similarly, light of the same wavelength appears periodically along the stripe, with spacing that varies depending on the spatial region. This behavior can be approximated using the theoretical calculations described in Xiao's work<sup>36</sup>. By introducing a properly configured blazed grating into the optical path, light of different wavelengths at the same vertical position is further separated horizontally, enabling the conversion of the one-dimensional spectrum into a two-dimensional spatial distribution. Before constructing the VIPA spectrometer, we conducted theoretical simulations and calculations, including modeling the system using Zemax to optimize the parameters of optical components. This ensured the spectrum could be compressed into as small a two-dimensional space as possible. As shown in Figure 2(a), light emitted from the fiber enters a reflective collimator (Thorlabs RC12FC-P01), which collimates the light from the single-mode fiber into a parallel beam with a diameter of approximately 13.2 mm. A cylindrical lens with a focal length of 200 mm focuses the beam onto the VIPA. The VIPA is made from fused silica, with a thickness of 1.68 mm, a size of 1 inch, an FSR of 61 GHz, a finesse of 71, and a wavelength range of 1500–1700 nm. The blazed grating has a groove density of 600

lines/mm, a blaze wavelength of 1550 nm, a blaze angle of  $26.78^\circ$ , and a size of 1 inch. The focusing lens has a focal length of 300 mm. The CCD used is the SWIR1300KMA, with a resolution of  $1280 \times 1064$  pixels and a pixel size of  $5.0 \mu\text{m} \times 5.0 \mu\text{m}$ . Using the VIPA design tool from LightMachinery, we found that the VIPA theoretically covers approximately 3.5 mm per FSR in the vertical direction. In the ideal case, each pixel corresponds to a bandwidth of 88.5 MHz, leading to a spectral resolution bandwidth of 0.86 GHz (about 10 pixels). The blazed grating, in the horizontal direction, provides a wavelength coverage of over 30 nm within a 6.4 mm range, with a theoretical spectral resolution of approximately 12.74 GHz, which exceeds one FSR of the VIPA. This design results in a VIPA spectrometer with a spectral resolution of approximately 860 MHz and a spectral coverage greater than 30 nm.

**Spectral Wavelength Calibration and Determination:** The frequency-modulated comb, which records the sample's absorption features, passes through the dispersion module composed of the VIPA and grating, and is imaged onto the CCD array. The resulting image is shown in the left panel of Figure 2(c). Each bright spot on the two-dimensional image corresponds one-to-one with a tooth of the frequency-modulated comb. The dispersion along the y-axis of the 2D image is determined by the dispersive capability of the VIPA, while the dispersion along the x-axis is determined by the dispersive capability of the grating. In this experiment, the DKS comb we generated has a repetition frequency of 19.98 GHz, and the free spectral range (FSR) of the VIPA used is 60 GHz. This determines that each tooth of the DKS comb will appear every three spots along the y-axis. Thus, in the left image of Figure 2(c), we observe three

rows of well-ordered spots. The direction of wavelength variation is shown in the right panel of Figure 2(c), with the white arrow indicating the direction of increasing wavelength. Consequently, the relationship between the spots in each row of the left image can be expressed as (from bottom to top):  $1+3N, 2+3N, 3+3N$  (where  $N=0,1,2,3,\dots$ ). To determine the precise wavelength of each spot, we replace the DKS comb source with a tunable single-frequency laser, tuning in steps of 0.02 nm. The CCD records the position of each bright spot at each wavelength, allowing the establishment of a one-to-one correspondence between the spots and wavelengths. Using this relationship, we can apply interpolation to map the wavelengths across the entire CCD, thus achieving the mapping between wavelength and CCD pixels. Since we use an electro-optic intensity modulator to generate the frequency-modulated comb, when the applied modulation frequency  $f_m$  is small, it causes the two bright spots in the CCD image to be too close together and thus indistinguishable. Therefore, in this experiment,  $f_m$  does not start from 0 Hz but instead increases from 1.5 GHz to 8.5 GHz. The blind spot in the frequency range can be addressed by adjusting the temperature of the microcavity (by raising or lowering it by approximately 2°C), which alters the pump wavelength of the single soliton. This shift in pump wavelength moves it by about 4 GHz (around 0.032 nm), allowing  $f_m$  to increase from 1.5 GHz to 8.5 GHz and regenerate the frequency-modulated comb, thus filling in the blind spot. Since the frequency-modulated comb can be expressed as  $f = f_p \pm nf_r \pm f_m$  ( $n \in 0,1,2,3,\dots$ ), where  $f_p$  is the frequency corresponding to the pump wavelength,  $f_r$  is the repetition frequency of the DKS comb, and  $f_m$  is the modulation frequency applied to the

electro-optic modulator, all of  $f_p$ ,  $f_r$ , and  $f_m$  are known throughout the process. This allows the calculation of the frequency of each tooth of the frequency-modulated comb. However, it is necessary to correspond the calculated comb tooth frequencies with the bright spots on the CCD. The one-to-one correspondence between the wavelength and CCD pixels has already been established, allowing us to approximate the frequency corresponding to each bright spot. The resolution error is limited by the finesse of the VIPA, but it is already higher than 1 GHz. When  $f_m$  increases from 1.5 GHz to 8.5 GHz in discrete steps, we can first determine the frequency of each bright spot on the CCD for  $f_m = 1.5\text{GHz}$  by directly matching the mapped frequency of the CCD bright spots with the frequency calculated from the formula. This allows us to correlate the intensity data collected by the CCD with the calculated frequencies. Subsequently, each stepwise increase of  $f_m$  can be calculated in the same way, thus achieving the calibration and determination of the frequency-modulated comb. Through this approach, the microwave frequency sweeping method with sub-Hz stability and accuracy can be converted to the optical frequency domain, significantly improving frequency precision, which ultimately depends on the linewidth of the frequency-modulated comb teeth and the accuracy of the repetition frequency.

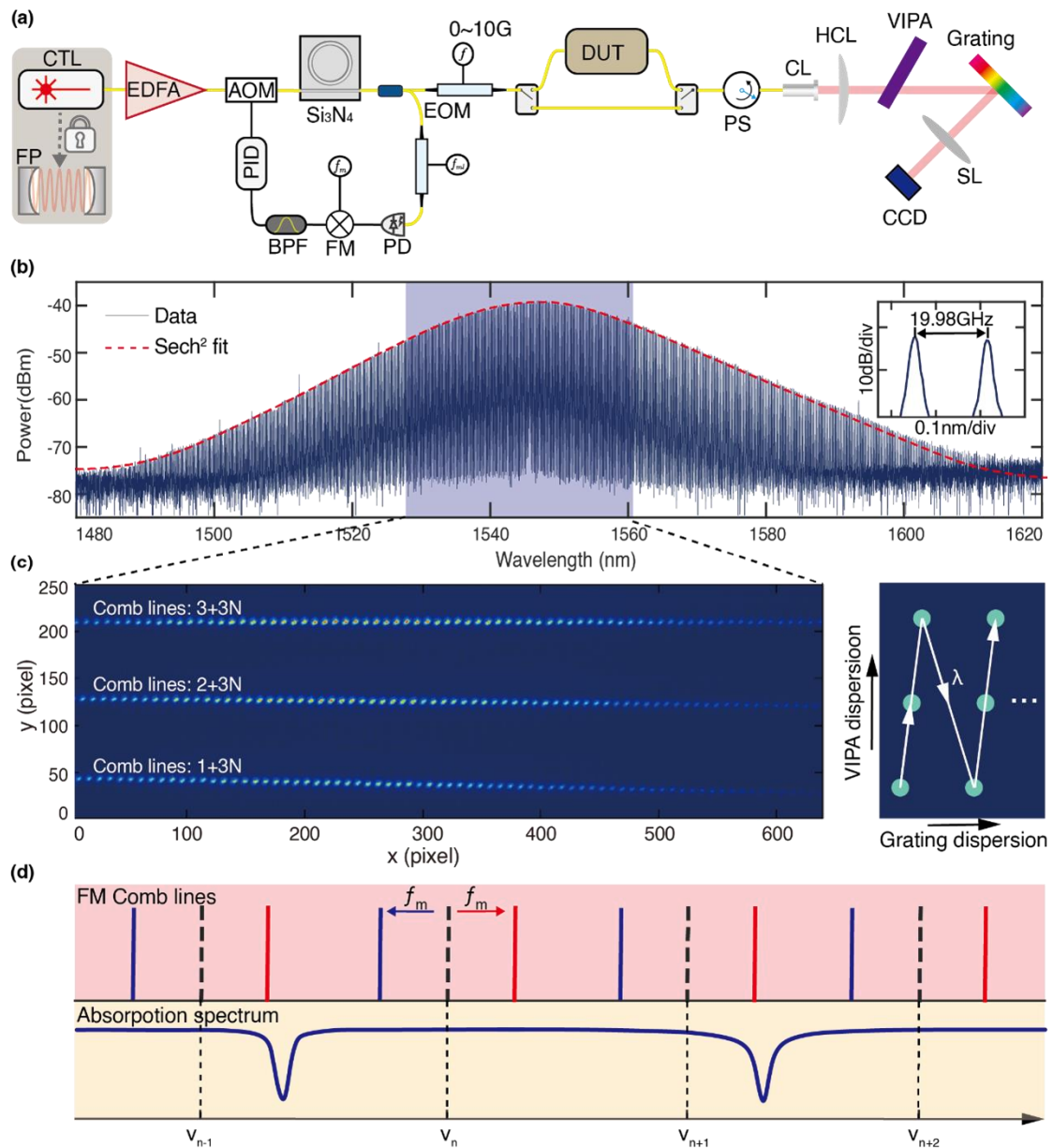


Fig. 2 Optical Layout of the Microcavity Transmission Spectrometer and Imaging of the DKS Optical Frequency Comb. (a) Optical Layout of the Microcavity Transmission Spectrometer. CTL: Continuously Tunable Laser; FP: Fabry-Pérot Cavity; EDFA: Erbium-Doped Fiber Amplifier; AOM: Acousto-Optic Modulator; PID: Proportional-Integral-Derivative Controller; BPF: Band-Pass Filter; FM: Frequency Mixer; PD: Photodetector; EOM: Electro-Optic Modulator; DUT: Device Under Test; PS: Polarization Scrambler; CL: Collimating Lens; SL: Spherical Lens; HCL: Cylindrical Lens. (b) Spectrometer Measurement Results of the DKS Optical Frequency Comb. The inset in the upper right corner displays

the measured results of two comb lines of the DKS optical frequency comb, with a repetition frequency of approximately 19.98 GHz. (c) Imaging of the DKS Optical Frequency Comb on a CCD Array(The left image shows the actual imaging of the DKS optical frequency comb on the CCD, while the right illustration demonstrates the dispersion directions of the grating and VIPA on the CCD, indicating the path and orientation of wavelengths from shorter to longer in the image). (d) Demonstration of the Principle for Extracting Gas Absorption Line Features Using Bidirectional Scanning of the DKS Optical Frequency Comb.

We used the microcavity transmission spectrometer to test three samples. The samples were sequentially placed at the position of the device under test in the optical setup shown in Figure 2(a), with one path of pure optical fiber serving as the reference. By controlling the frequency applied to the EOM, we performed frequency sweeping with different step intervals, thereby generating optical frequency combs with different repetition rates. During the sweeping process, optical switches were used in real-time to obtain synchronized reference spectral data, which were then used for normalization in absorption spectrum measurements. The test results are shown in Figure 3. The repetition frequencies of the combined frequency combs vary across the three samples, depending on the absorption linewidth of the samples. Figures 3(a) and (b) show the results for HCN gas. We used an HCN gas cell with a pressure of 25 torr and an optical path length of 16 cm, considering that the absorption linewidth of HCN gas at normal temperature is approximately 2 GHz. We conducted the test with a step interval of 50 MHz, resulting in a combined frequency comb repetition rate of 50 MHz. The measurement time for each scan was approximately 3 seconds. The measurement time



in this setup is limited by the frequency switching time of the microwave signal generator (1 ms) and the frame rate of the camera (approximately 130 Hz at its fastest). However, these limitations can be improved in the future to achieve shorter measurement times. Figure 3(a) shows the normalized absorption spectrum of HCN gas measured over a wavelength range of 1526–1562 nm, spanning 34 nm. Figure 3(b) presents a magnified view of the absorption line of HCN at 1554.56 nm, which is fitted using a Voigt function. The Lorentzian FWHM linewidth obtained from the fit is 2 GHz, consistent with the manufacturer’s reported linewidth of 16 pm (approximately 1.997 GHz) for the gas cell. As shown in Figure 3(a), our method enables broadband spectral measurements spanning 34 nm (approximately 4 THz). The spectral bandwidth is primarily constrained by the optical design of the backend free-space optical path. Utilizing lenses with shorter focal lengths can facilitate even broader spectral measurements. To further validate the analytical capability of the microresonator transmission spectrometer, we tested an encapsulated silicon nitride microresonator, with results shown in Figures 3(c) and 3(d). The mode spacing of the microresonator is approximately 35 GHz, and the linewidth is about 27 MHz. Therefore, measurements were conducted with a step size of 1 MHz, resulting in a composite frequency comb with a repetition frequency of 1 MHz. Figure 3(c) illustrates the absorption spectrum of the silicon nitride microresonator over a 34 nm range from 1526 to 1562 nm. Figure 3(d) shows a magnified view of an absorption line at 1545.35 nm, fitted with a Lorentzian function, yielding a full-width at half-maximum (FWHM) linewidth of 27 MHz. These results demonstrate that our method achieves spectral resolution better

than 1 MHz over a wide spectral range. To explore the detection limits of this approach, we also measured the absorption spectrum of a whispering-gallery-mode (WGM) cylindrical resonator with an extremely high Q-factor. The results are shown in Figures 3(e) and 3(f). The WGM resonator exhibits irregular mode spacing but features extremely narrow absorption lines due to its high Q-factor, with linewidths as narrow as 1 MHz. Considering the 200 kHz linewidth of the CTL laser used in the experiment, measurements were performed with a step size of 200 kHz. Figure 3(f) presents an absorption line with a linewidth of approximately 1 MHz. These findings demonstrate that the microresonator transmission spectrometer can resolve ultranarrow absorption lines, providing richer spectral details for precise analysis.

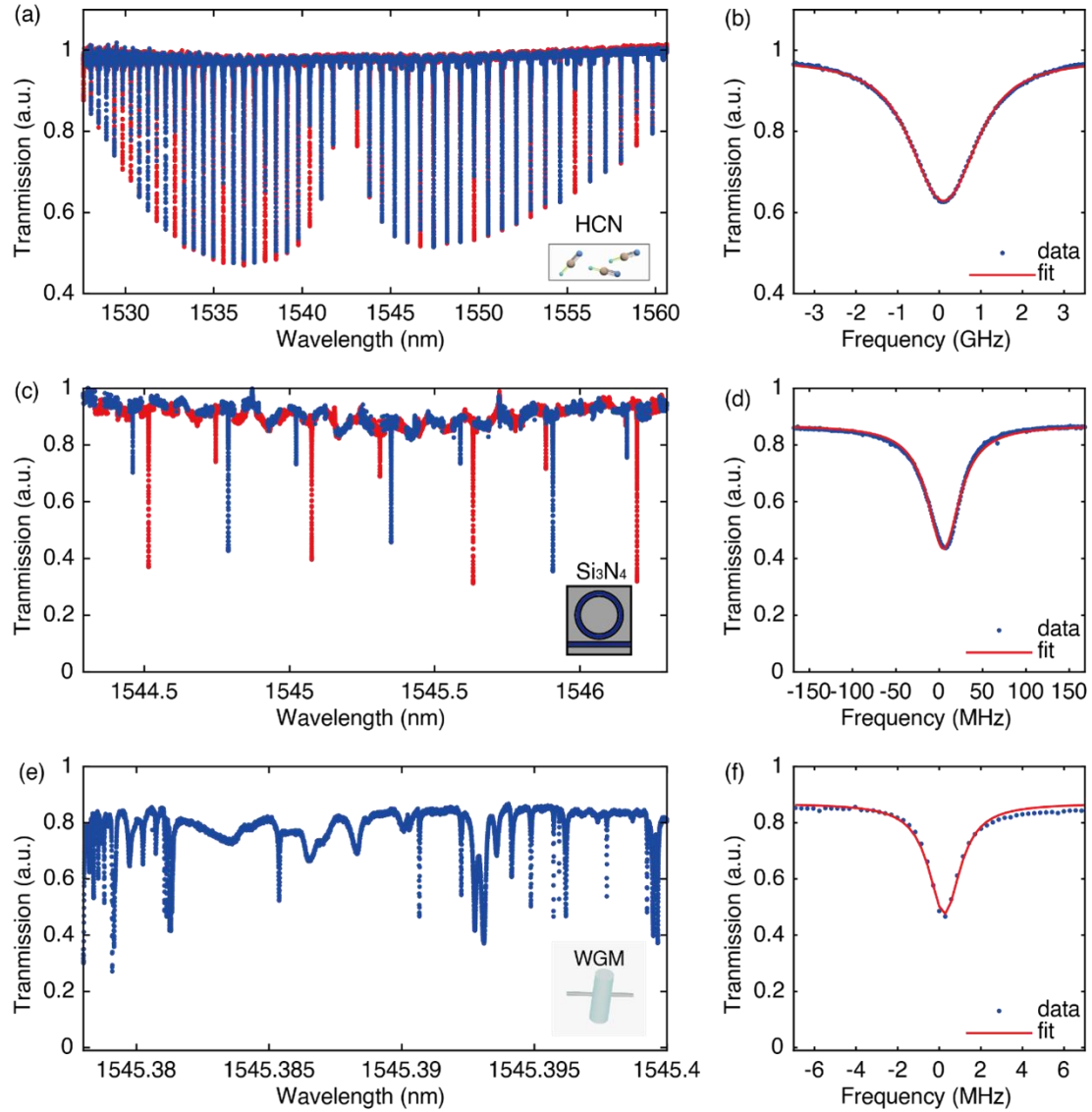


Fig. 3 Spectral Measurement Results of Three Samples (HCN Gas Cell, Silicon Nitride Microcavity, and WGM Cylindrical Cavity) Using the Microcavity Transmission Spectrometer. (a) and (b): Spectral measurement results of the HCN gas cell. Panel (b) corresponds to the absorption line at 1554.56 nm in panel (a), with a linewidth of approximately 2 GHz. (c) and (d): Spectral measurement results of the silicon nitride microcavity. Panel (d) corresponds to the transmission absorption feature at 1545.35 nm in panel (c), with a linewidth of approximately 35 MHz. (e) and (f): Spectral measurement results of the WGM cylindrical cavity. Panel (f) corresponds to the transmission absorption feature at 1545.3957 nm, with a linewidth of approximately 2 MHz.

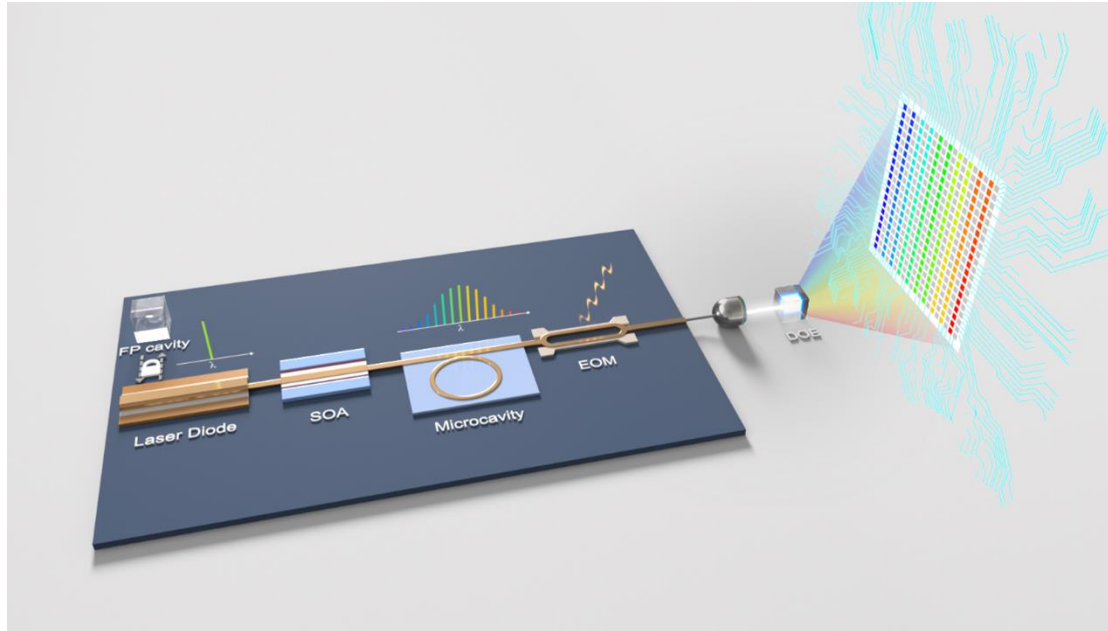


Fig. 4 Integrated Microcavity Transmission Spectrometer. The core components of the microcavity transmission spectrometer, including the laser source, silicon nitride microcavity, and electro-optic modulator, can be integrated on-chip. SOA: Semiconductor Optical Amplifier; DOE: Diffractive Optical Element.

## Discussion

In conclusion, we have demonstrated a microcavity transmission spectrometer based on a single silicon nitride microcavity soliton, offering a 4 THz bandwidth and a resolution of up to 200 kHz. The stable dissipative Kerr soliton (DKS) comb, combined with the double-sideband fast sweeping capability of the intensity electro-optic modulator (EOM), effectively transfers the sub-Hz precision of the radio frequency (RF) domain to the optical domain. The resulting frequency-modulated comb inherits high-precision characteristics from the RF source, with its frequency accuracy dominated by the precision of the pump laser and the stability of the repetition rate. By locking the pump laser to a stable Fabry-Pérot (FP) cavity and referencing the DKS comb's

repetition rate to a highly accurate RF source (e.g., a stable crystal oscillator), an ultrahigh-precision frequency-modulated comb was achieved. This comb was analyzed using a VIPA coupled with a diffraction grating to project the spectrum onto a two-dimensional CCD array. By continuously recording the frequency-modulated comb spectrum during the fast sweeping process, a composite spectrum was obtained in a short time. Moreover, the method preserves the sub-Hz precision characteristics of the RF domain throughout the scanning process. With an ultra-narrow-linewidth pump laser locked to an ultra-stable cavity and the repetition rate passively stabilized, precision and stability at the Hz level could potentially be achieved. Additionally, the key components of this system such as the pump laser, FP cavity, microresonator, EOM, and SOA are inherently suitable for integration, as shown in Figure 4. This approach holds significant potential for miniaturization and integration, making it highly promising for compact, high-precision spectral measurement applications.

## **Acknowledgments**

This research was supported by National Natural Science Foundation of China (42125402); The B-type Strategic Priority Program of CAS (XDB0780000); National Natural Science Foundation of China (Grant No. 42188101, 92476112, 42374185, 12261131503, 12404436); Innovation Program for Quantum Science and Technology (2021ZD0300301, 2023ZD0301500); Guangdong-Hong Kong Technology Cooperation Funding Scheme (Grant No. 2024A0505040008); Shenzhen-Hong Kong Cooperation Zone for Technology and Innovation (HZQB-KCZYB2020050);

Shenzhen Science and Technology Program (Grant No. RCJC20231211090042078); State Key Laboratory of Pulsed Power Laser Technology Foundation; Furthermore, ZRC is grateful for the support from USTC Tang Scholar; XXH is grateful for the support from the New Cornerstone Science Foundation through the XPLOER PRIZE.

### **Conflict of interest**

C. S. and J. Liu are co-founders of Qaleido Photonics, a start-up that is developing heterogeneous silicon nitride integrated photonics technologies. Others declare no competing interests.

**Supplementary information.** See supplement information for supporting content.

### **References**

1. Schiller, S. Spectrometry with frequency combs. *Optics letters* **27**, 766–768 (2002).
2. Coddington, I., Swann, W. C. & Newbury, N. R. Coherent multiheterodyne spectroscopy using stabilized optical frequency combs. *Physical review letters* **100**, 013902 (2008).
3. Zhu, F. *et al.* Real-time dual frequency comb spectroscopy in the near infrared. *Applied Physics Letters* **102**, (2013).
4. Rieker, G. B. *et al.* Frequency-comb-based remote sensing of greenhouse gases over kilometer air paths. *Optica* **1**, 290–298 (2014).
5. Cingöz, A. *et al.* Direct frequency comb spectroscopy in the extreme ultraviolet.

*Nature* **482**, 68–71 (2012).

6. Gohle, C. *et al.* A frequency comb in the extreme ultraviolet. *Nature* **436**, 234–237 (2005).

7. Pupeza, I., Zhang, C., Högner, M. & Ye, J. Extreme-ultraviolet frequency combs for precision metrology and attosecond science. *Nature Photonics* **15**, 175–186 (2021).

8. Schliesser, A., Picqué, N. & Hänsch, T. W. Mid-infrared frequency combs. *Nature photonics* **6**, 440–449 (2012).

9. Jerez, B., Martín-Mateos, P., Prior, E., de Dios, C. & Acedo, P. Dual optical frequency comb architecture with capabilities from visible to mid-infrared. *Optics Express* **24**, 14986–14994 (2016).

10. Liu, J. *et al.* Ultralow-power chip-based soliton microcombs for photonic integration. *Optica* **5**, 1347–1353 (2018).

11. Shen, B. *et al.* Integrated turnkey soliton microcombs. *Nature* **582**, 365–369 (2020).

12. Liu, J. *et al.* Photonic microwave generation in the X-and K-band using integrated soliton microcombs. *Nature Photonics* **14**, 486–491 (2020).

13. Wan, S. *et al.* Frequency stabilization and tuning of breathing solitons in Si<sub>3</sub>N<sub>4</sub> microresonators. *Photonics Research* **8**, 1342–1349 (2020).

14. Pu, M., Ottaviano, L., Semenova, E. & Yvind, K. Efficient frequency comb generation in AlGaAs-on-insulator. *Optica* **3**, 823–826 (2016).

15. Sun, Y. *et al.* Ultrahigh Q microring resonators using a single-crystal aluminum-nitride-on-sapphire platform. *Optics letters* **44**, 5679–5682 (2019).

16. Wilson, D. J. *et al.* Integrated gallium phosphide nonlinear photonics. *Nature*

*Photonics* **14**, 57–62 (2020).

17. Hausmann, B., Bulu, I., Venkataraman, V., Deotare, P. & Lončar, M. Diamond nonlinear photonics. *Nature Photonics* **8**, 369–374 (2014).

18. He, Y. *et al.* Self-starting bi-chromatic LiNbO<sub>3</sub> soliton microcomb. *Optica* **6**, 1138–1144 (2019).

19. Newman, Z. L. *et al.* Architecture for the photonic integration of an optical atomic clock. *Optica* **6**, 680–685 (2019).

20. Papp, S. B. *et al.* Microresonator frequency comb optical clock. *Optica* **1**, 10–14 (2014).

21. Suh, M.-G., Yang, Q.-F., Yang, K. Y., Yi, X. & Vahala, K. J. Microresonator soliton dual-comb spectroscopy. *Science* **354**, 600–603 (2016).

22. Trocha, P. *et al.* Ultrafast optical ranging using microresonator soliton frequency combs. *Science* **359**, 887–891 (2018).

23. Riemensberger, J. *et al.* Massively parallel coherent laser ranging using a soliton microcomb. *Nature* **581**, 164–170 (2020).

24. Lucas, E. *et al.* Ultralow-noise photonic microwave synthesis using a soliton microcomb-based transfer oscillator. *Nature communications* **11**, 374 (2020).

25. Diddams, S. A., Hollberg, L. & Mbele, V. Molecular fingerprinting with the resolved modes of a femtosecond laser frequency comb. *Nature* **445**, 627–630 (2007).

26. Waxman, E. M. *et al.* Intercomparison of open-path trace gas measurements with two dual-frequency-comb spectrometers. *Atmospheric measurement techniques* **10**, 3295–3311 (2017).



27. Yu, M., Okawachi, Y., Griffith, A. G., Lipson, M. & Gaeta, A. L. Microresonator-based high-resolution gas spectroscopy. *Optics letters* **42**, 4442–4445 (2017).
28. Yu, M. *et al.* Gas-phase microresonator-based comb spectroscopy without an external pump laser. *Acs Photonics* **5**, 2780–2785 (2018).
29. Kuse, N., Tetsumoto, T., Navickaite, G., Geiselmann, M. & Fermann, M. E. Continuous scanning of a dissipative Kerr-microresonator soliton comb for broadband, high-resolution spectroscopy. *Optics Letters* **45**, 927–930 (2020).
30. Niu, R. *et al.* Fast spectroscopy based on a modulated soliton microcomb. *IEEE Photonics Journal* **13**, 1–4 (2021).
31. Zhu, X. & He, J. Numerical study of comb-based high-accuracy distance measurement utilizing VIPA interferometry. *Journal of Optics* **21**, 025703 (2019).
32. Bao, C., Suh, M.-G. & Vahala, K. Microresonator soliton dual-comb imaging. *Optica* **6**, 1110–1116 (2019).
33. Qing, T. *et al.* Vector spectrometer with Hertz-level resolution and super-recognition capability. *arXiv preprint arXiv:2402.09752* (2024).
34. Weng, W. *et al.* Spectral purification of microwave signals with disciplined dissipative Kerr solitons. *Physical review letters* **122**, 013902 (2019).
35. Guo, H. *et al.* Universal dynamics and deterministic switching of dissipative Kerr solitons in optical microresonators. *Nature Physics* **13**, 94–102 (2017).
36. Xiao, S., Weiner, A. M. & Lin, C. A dispersion law for virtually imaged phased-array spectral dispersers based on paraxial wave theory. *IEEE journal of quantum electronics* **40**, 420–426 (2004).

36. Shi, B. et al. Frequency-comb-linearized, widely tunable lasers for coherent ranging. *Photon. Res.* 12, 663-681 (2024).
37. Ye, Z. et al. Foundry manufacturing of tight-confinement, dispersion-engineered, ultralow-loss silicon nitride photonic integrated circuits. *Photon. Res.* 11, 558-568 (2023).
38. Sun, W. et al. A chip-integrated comb-based microwave oscillator. *arXiv* 2403.02828 (2024).

# Supplemental Instrument for a High-resolution Microcavity Transmission Spectrometer

Ruocan Zhao<sup>1†</sup>, Bin Yang<sup>1†</sup>, Chuan Huang<sup>1</sup>, Jiangtao Li<sup>1</sup>, Baoqi Shi<sup>3</sup>, Wei Sun<sup>3</sup>, Chen Shen<sup>3,4</sup>, Chong Wang<sup>1</sup>, Tingdi Chen<sup>1,2</sup>, Chen Liang<sup>2</sup>, Xianghui Xue<sup>1,2,5,6</sup>, Junqiu Liu<sup>2,3</sup>, Xiankang Dou<sup>2</sup>

\*Corresponding author. Email: [xuexh@ustc.edu.cn](mailto:xuexh@ustc.edu.cn)

1. CAS Key Laboratory of Geospace Environment, School of Earth and Space Sciences, University of Science and Technology of China, Hefei 230026, China

2. Hefei National Laboratory, University of Science and Technology of China, Hefei 230088, China

3. International Quantum Academy, Shenzhen 518048, China

4. Qaleido Photonics, Shenzhen 518048, China

5. CAS Center for Excellence in Comparative Planetology, Anhui Mengcheng Geophysics National Observation and Research Station, University of Science and Technology of China, Hefei, China

6. Hefei National Research Center for Physical Sciences at the Microscale and School of Physical Sciences, University of Science and Technology of China, Hefei, China.

†These authors contributed equally to this work

## 1. Characterization of the Microcavity and DKS Repetition Rate Stability Test

We used a vector spectrometer to measure the transmission spectrum of the microcavity (TE mode) from 1480 nm to 1640 nm and computed the corresponding dispersion curve. The dispersion is described using the relation  $D_{\text{int}}(\mu) = \frac{D_2}{2!} \mu^2 + \frac{D_3}{3!} \mu^3 + \dots$ , and polynomial fitting was performed to obtain the values of  $D_2, D_3, \dots$ . The microcavity dispersion characterization and measurement results are shown in Figure S1(a). Figures S1(c) and (d) show the characterization of the soliton's quality factor (Q factor) and the time-domain response of the pump light scanning the microcavity at 800 mW power, with the soliton step broadened via EOM modulation. As observed, after modulation by the EOM, the soliton step width is 200 MHz. Additionally, to achieve repetition rate locking of the soliton, a separate path was extracted from the microcavity output for soliton locking. The output light first passes through an intensity-modulated EOM, and the beat frequency signal is captured by a high-speed photodetector (PD). The RF frequency is then applied to the phase modulation for locking. Here,  $f_{ml} = (f_r - f_m)/2$  where  $f_r$  is the DKS soliton's repetition rate, and  $f_m$  is the reference frequency for locking. Both  $f_m$  and  $f_{ml}$  can be traced to an accurate rubidium atomic clock. The beat frequency signal is mixed with a signal at frequency  $f_m$ , filtered through a low-pass filter, and then fed back to the acousto-optic modulator (AOM) through a PID loop. By adjusting the power input to the microcavity, the DKS soliton's

repetition rate is locked. Figure S1(e) shows the results of the DKS soliton repetition rate lock, as measured using a spectrum analyzer.

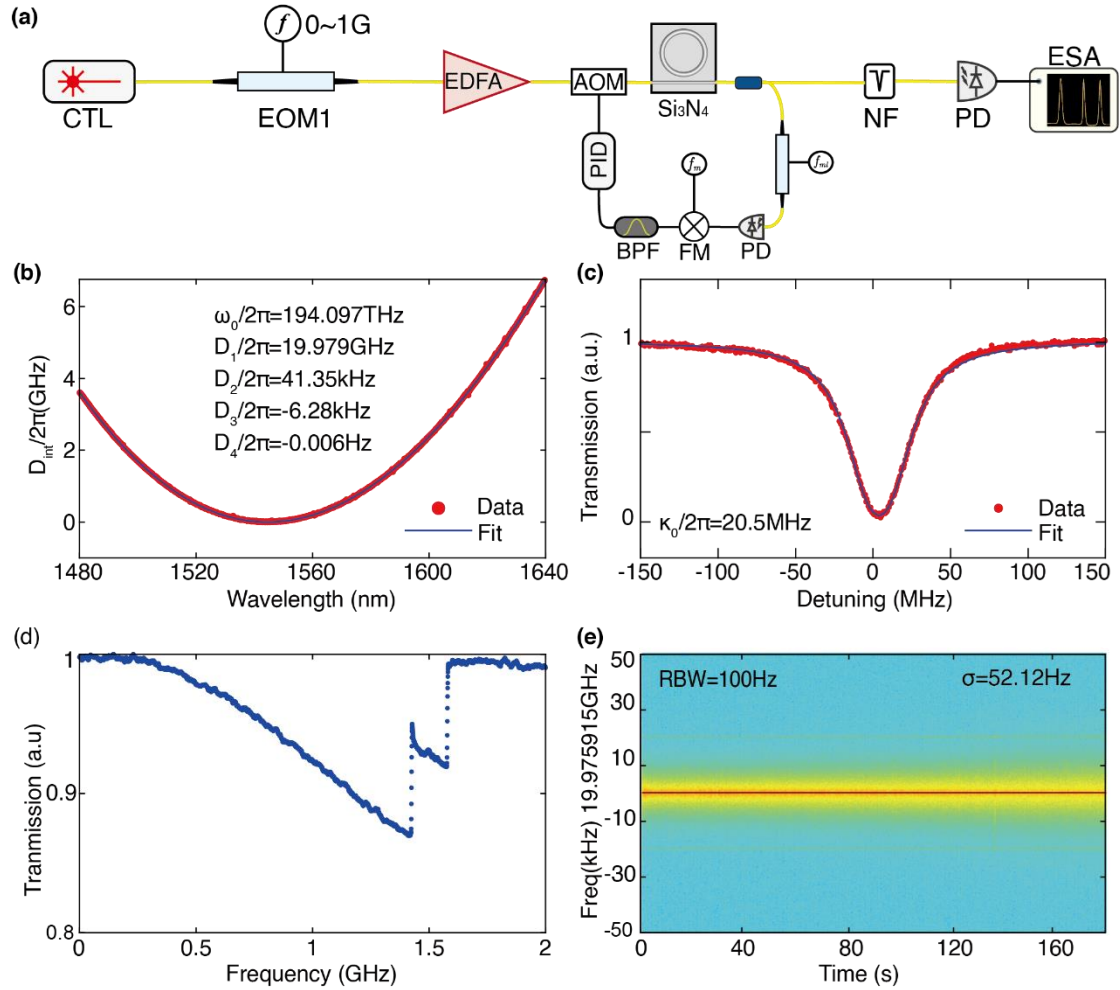


Fig. S1 DKS Comb Repetition Rate Measurement and Microcavity Characterization. (a) Schematic of the DKS comb repetition rate measurement. NF: Notch filter; ESA: Electrical spectrum analyzer. (b) Dispersion distribution and fitting of the integrated microcavity. (c) Resonant transmission measurement of the microcavity. (d) Time-domain response during pump light scanning of the microcavity. (e) DKS comb repetition rate measurement results.

## 2. Pump light Locking

The spectral accuracy of the microcavity transmission spectrometer is not only dependent on the DKS repetition rate but also on the pump light. For the DKS comb,

the role of the pump light is similar to the initial frequency (carrier-envelope offset frequency) in a mode-locked comb, determining the overall offset of the DKS comb. To improve the frequency accuracy of the DKS comb, although additional locking of the pump light is required, it also provides an absolute reference for the DKS comb. In this work, we use the Pound-Drever-Hall (PDH) technique to lock the pump light to a high-stability FP cavity. The optical setup is shown in Fig. S2(a). After emission from the CTL laser, the pump light is split into two paths using a beam splitter. One path is mixed with the mode-locked comb locked to the ultra-stable cavity and then filtered through a bandpass filter. The signal is detected by a high-speed photodetector (PD) and sent to a spectrum analyzer to monitor the stability of the pump light. The other path is modulated by a phase EOM (0-1 GHz) and then converted into spatial light, subsequently passing through a polarizing beam splitter (PBS) and entering the FP cavity to obtain its reflection absorption spectrum. The reflected light is then reflected back through the PBS and a mirror before entering the high-speed PD. The electrical signal from the reflected light is phase-demodulated to generate an error signal, which is fed back via a PID controller to the CTL laser for frequency compensation, achieving the locking of the pump light. Fig. S2(b) shows the result of the beat frequency between the pump light and the mode-locked comb locked to the ultra-stable cavity after locking the pump light. It can be seen that the linewidth of the pump light is less than 200 kHz. Fig. S2(c) shows the long-term stability test of the pump light, measured by the beat frequency with the mode-locked comb after the pump light is locked.

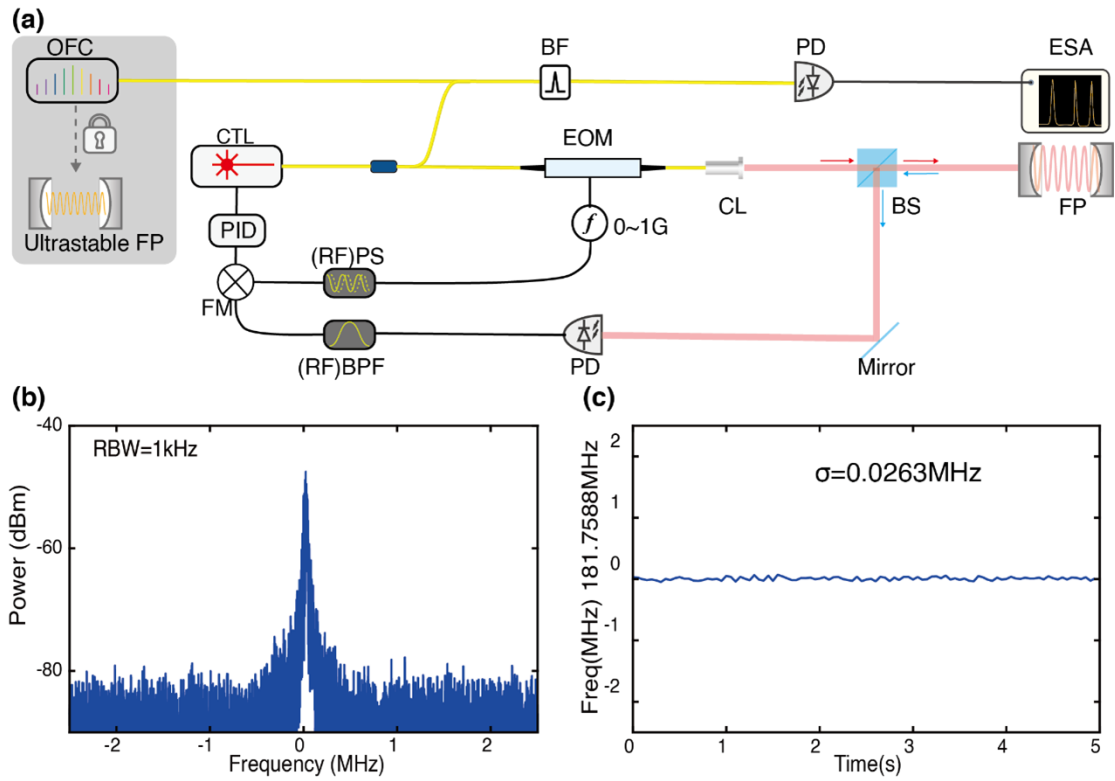


Fig. S2 Pump Light Locking and Measurement. (a) Schematic of pump light locking. PBS: Beam splitter; PS: Phase shifter. (b) Beat frequency result of pump light after locking with the mode-locked comb (locked on ultra-stable laser). (c) Stability measurement result of pump light after locking.

### 3. HCN Measurement Results of the Microcavity Transmission Spectrometer and Comparison with the HITRAN Database.

Fig S3(a) Comparison of HCN gas measurement results using the microcavity transmission spectrometer with the HCN data from the HITRAN database, demonstrating the frequency accuracy of the spectrometer. (b) Measured and fitted curve of one of the absorption lines after amplification.

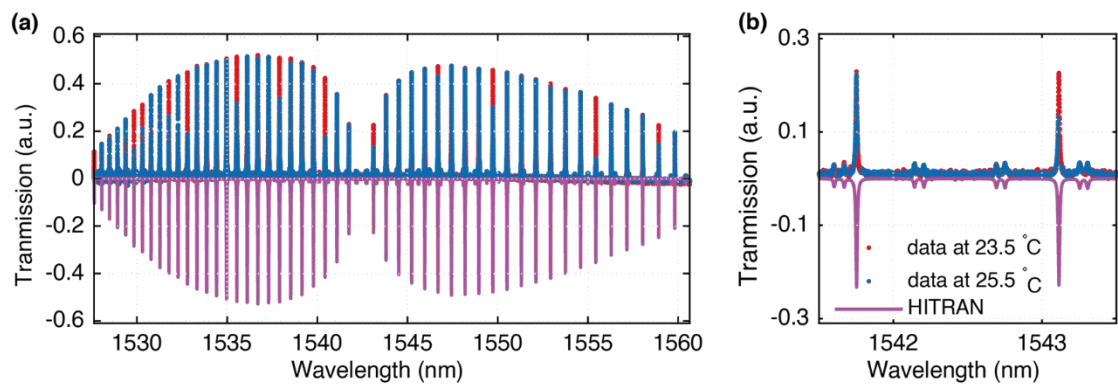


Fig. S3 Comparison of HCN Gas Measurements from the Microcavity Transmission Spectrometer with the HITRAN Database. (a) Direct comparison of HCN gas measurement results from the microcavity transmission spectrometer with the HITRAN database. (b) Enlarged view of absorption line at 1542.5nm.